Chapter 10

WIND PATTERNS IN THE WESTERN DESERT

FAROUK EL-BAZ and R. W. WOLFE
National Air and Space Museum
Smithsonian Institution
Washington, D.C. 20560

ABSTRACT

The Western Desert is part of the driest region on Earth, where the incident solar radiation is capable of evaporating 200 times the amount of precipitation. For this reason wind is the main agent of erosion and deposition in a completely eolian environment. Data on wind velocity and direction are analyzed in this paper to establish their relationships to sand transport and orientation of dunes. Surface wind data are summarized for 42 meteorological stations between 15° and 35° N latitude and 15° and 41° E longitude. The summaries are presented in the form of graphs showing the patterns of sand-moving winds in wind roses, sand-drift potential in resultants, and streamlines. The basic patterns agree with the overall southward direction of prevailing wind, and thus of general sand transport directions. Variations from this general pattern are believed to be due to interaction between the wind and local topography. Prevailing wind directions in the Western Desert are also analyzed in terms of seasonal wind circulation patterns in North Africa. Because of the scarcity of data, it is recommended that automated meteorological stations be used to gather information on local winds in the open desert, particularly in the southwestern part, which is important for analog correlations with Mars.

INTRODUCTION

As part of the eastern Sahara, the Western Desert is one of the driest places on Earth. The "aridity index" of much of this desert is 200, which means that the incident solar energy is capable of evaporating 200 times the amount of precipitation received (Henning and Flohn, 1977). Because of this extreme aridity, wind is the main agent of sculpture in this desert. Wind, air moving more or less parallel to the surface of the ground, dismantles scarps, deepens hollows and erodes exposed rocks. The products of erosion are either hurled in the atmosphere as dust, accumulated in the form of sand sheets and dunes, or are left behind as coarse lag deposits.

Thus, an understanding of the prevailing wind directions and their variations is necessary to the study of eolian depositional and erosional features of this desert. In this paper we present a preliminary analysis of the available wind data and their relations to known directions of sand dunes.

Much of the basic research on dune classifications and sand movement has been carried out in the Western Desert. Based on his observations in this desert, Bagnold (1933; 1941; Bagnold and others, 1939) charted the major dune locations and discovered the basic principles of sand transport by wind. He attributed the main direction of dunes to a clockwise circulation of wind about a center near the Kufra Oasis in southeastern Libya.

Bagnold's early observations have recently been supported by studies of sand dune patterns as revealed by photographs taken from space (Fig. 10.1). Gifford and others (1979, p. 219) established that "the dune orientations change from north-northwesterly in the northern desert to north-northeasterly in the south. The dunes are intimately associated with scarps that bound numerous depressions in the Western Desert. This relationship is believed to result from the interactions between sand-carrying winds and scarps and other topographic variations."

A preliminary investigation of sand-moving winds from 21 stations in Egypt by Wolfe and El-Baz (1979, p. 299) revealed two major wind regimes: "a narrow band of predominantly westerlies along the Mediterranean seacoast and generally north-northwesterlies throughout the Western Desert. Imposed upon these regional trends are local variations that may be attributed to topographic effects."

It is important to note here that the northeasterly trend observed on the basis of dune orientations (Gifford and others, 1979) did not show up in the wind data analysis by Wolfe and El-Baz (1979). This is basically due to the lack of wind recording stations in the southwestern part of the desert, where the dunes veer towards a northeasterly orientation. In other localities, dune orientations were found to mimic prevailing wind direction. For this reason, the local topographic setting of meteorological stations in the Western Desert must be considered when using the wind data.

The wind data used in this study were obtained from the U.S. National Climatic Center in the form of U.S. Air Force N-type summaries (Summary Form 2 - surface winds). These summaries were produced from observations by World Meteorological Organization (WMO) stations, and cover periods ranging from 7 to 13 years.

GENERAL WIND CIRCULATION

The wind circulation of northern Africa including the Western Desert of Egypt is influenced by many factors, especially the presence of seasonally semi-permanent high pressure areas and the location of the Inter-Tropical Convergence Zone (I.T.C.Z.), a discontinuity separating southeasterly and northeasterly winds (Griffiths and Soliman, 1972). The location of the I.T.C.Z. generally follows the path of the Sun with the advance of the seasons (Fig. 10.2) and may play the greatest role in determining the winds of southern Egypt and the Western Desert.

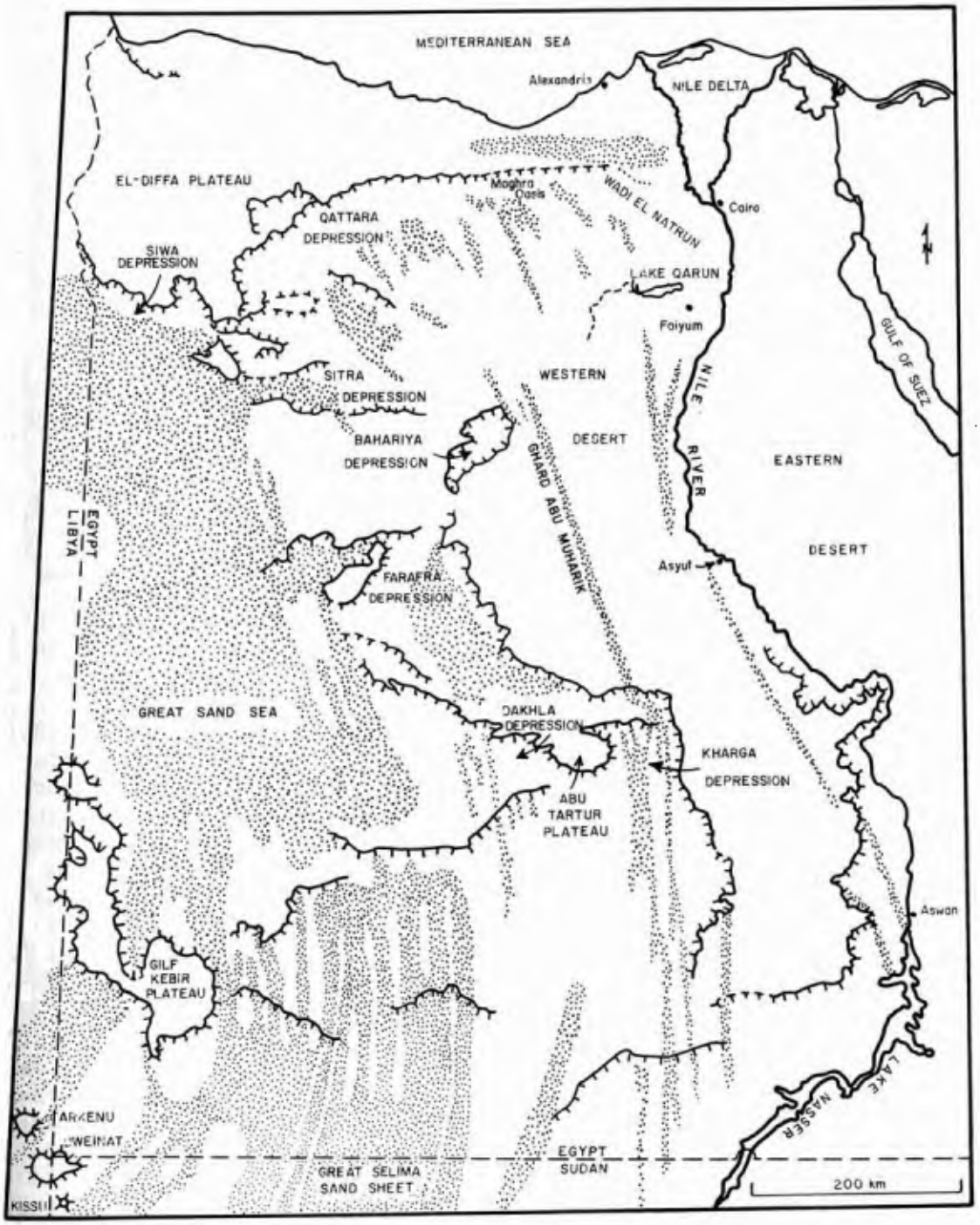

Figure 10.1 Sand dune belts of the Western Desert of Egypt as mapped from Apollo-Soyuz photographs and Landsat images. (Modified from Gifford and others, 1979, p. 225).

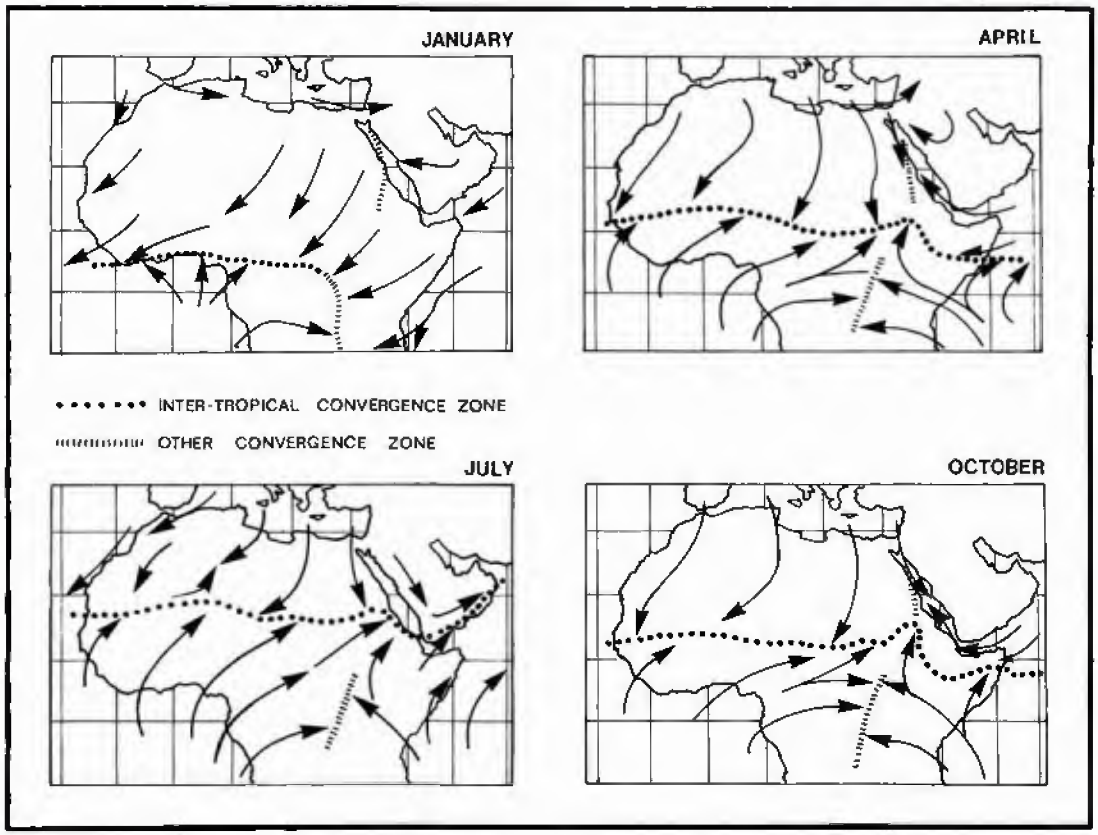

Figure 10.2 Wind circulation in North Africa as indicated by four months representing the seasons (After Griffiths and Soliman, 1972).

1. Winter (December-February): During this season, the I.T.C.Z. is far to the south and wind circulation is dominated by the presence of the large Saharan high situated in the western Sahara and modified by the passage of depressions across the Mediterranean Sea in northern Egypt. The winds, then, are generally north-northwesterly. In northern Egypt, winds are south-southwesterly in advance of the Mediterranean depressions and become northwesterly as the depressions pass. These two wind regimes are clearly seen in the wind map for January (Fig. 10.2).

2. Spring (March-May): During these months, the I.T.C.Z. begins to move northward (Fig. 10.2) and depressions become less frequent and follow tracks that are more southerly than in winter. Often these depressions are accompanied by strong southerly winds and may cause severe sandstorms.

3. Summer (June-September): The I.T.C.Z., which reaches its northerly limit during July, is located in northern Sudan (Fig. 10.2). During this season winds are generally northerly, even in northern Egypt. Generally, winds are stronger, blow more frequently, and are less variable than in other seasons.

4. Autumn (October-November): Like Spring, Autumn is a transition season with the I.T.C.Z. retreating southward. This retreat is more rapid than the Spring advance. With the exception of Aswan, this is the season of lowest wind speed (Griffiths and Soliman, 1972).

INTERACTIONS OF WIND AND SAND

Wind Data

Surface wind summaries for 42 observing stations between 15° and 35°N and 15° and 41°E listed in Table 10.1 were selected for analysis (Fig. 10.3). Of these, half (21 stations) are in Egypt, including the Sinai Peninsula. Only 9 stations cover parts of the Western Desert including eastern Libya, but none are located in the southern and southwestern parts of the desert. A guide to these and other weather summaries for the entire world is given by Ownbey (1978).

No details about the placement of anemometers or frequency and resolution of observation are included in the N-type summaries. However, World Meteorological Organization guidelines (WMO, No. 8 TPB)

Table 10.1. Name and designation of 42 wind stations whose data were studied in this report. See locations in Figure 10.3.

STATION	WMO No.	STATION	WMO No.
1. Abu Hamed	62640	22. Gulf of Suez	RS012
2. Abu Suer	62438	23. Helwan	62378
3. Agedabia	62055	24. Jeddah	40477
4. Alexandria	62318	25. Jerusalem	40184
5. Aswan	62414	26. Kassala	62370
6. Atbara	62680	27. Kharga	62435
7. Badanah	40357	28. Khartoum	62721
8. Bahariya	62420	29. Kufra	62271
9. Benina	62053	30. Luxor	62405
10. Cairo	62366	31. Manqabad	62393
11. Dakhla	62432	32. Mersa Matruh	62306
12. Derna	62059	33. Port Said	62333
13. Eilat	40199	34. Port Sudan	62641
14. El-Adem	62063	35. Quseir	62465
15. El-Arish	62336	36. Red Sea North	RS011
16. El-Tor	62459	37. Salum	62300
17. Faiyum	62318	38. Siwa	62417
18. Farafra	62423	39. Suez	62450
19. Gaza	62338	40. Tanta	62438
20. Gialo	62161	41. Turaif	40356
21. Giarabub	62176	42. Wadi Halfa	62600

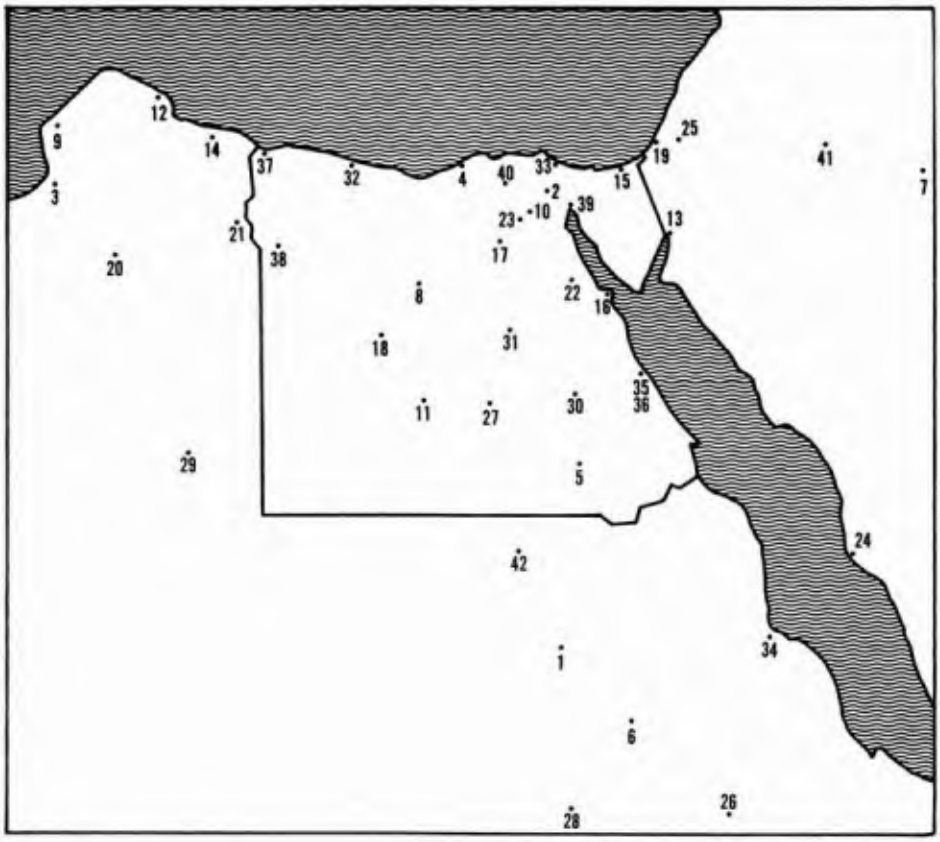

Figure 10.3 Location map of 42 wind stations from which data were analyzed (See Table 10.1 for name and number of individual stations).

recommend placement of anemometers 10 m above the surface and recording winds to the nearest one knot and to the nearest 10° direction. The data are summarized by month (in some cases an annual summary is available) and presented as frequency of occurrence in 15 (sometimes 8) directional classes corresponding to points of the compass, and 5 to 9 velocity classes shown in Table 10.2. Calm and variable winds are tallied separately.

Sand-Moving Winds

The basic expressions for the movement of sand by wind were developed by Bagnold (1941) based on field and laboratory observations. He assumed that a sand particle at rest would be about to move when the force of wind on the particle equaled the particle weight. The static threshold drag velocity, V_* describes these conditions, and is given by:

$$V_* = A \left(\frac{\rho_p - \rho_f}{\rho_f} \; g \; d \right)^{1/2} \qquad (1)$$

Table 10.2 Wind velocity classifications in WMO data.

5 Classes	9 Classes	
1 - 6 knots 0.5-3.1 m/sec	1 - 3 0.5-1.5	4 - 6 knots 2.1-3.1 m/sec
7 - 17 knots 3.6-8.2 m/sec	7 - 10 3.6-5.1	11 - 16 knots 5.7-8.2 m/sec
17 - 27 knots 8.7-13.9 m/sec	17 - 21 8.7-10.8	22 - 27 knots 11.3-13.9 m/sec
28 - 40 knots 14.4-20.6 m/sec	28 - 33 14.4-17.0	34 - 40 knots 17.5-20.6 m/sec
> 40 knots > 20.6 m/sec	> 40 knots > 20.6 m/sec	

where A is a constant; p, particle density; f, fluid (air) density; g, acceleration of gravity; and d, particle diameter. For medium sand (0.25 mm), the threshold drag velocity is about 0.22 m/sec. Once sand has begun to flow, the drag velocity decreases to 0.19 m/sec., which is called the dynamic threshold drag velocity, V_*' (Bagnold, 1941).

The wind velocity, v, at any height, z, near the surface can be related to the threshold drag velocity by:

$$v = 5.75\ V_* \log z/k \qquad (2)$$

where k is the height below which the velocity is zero. This height is related to the roughness of the surface and is approximately equal to 1/30 of the diameter of grains making up the ground surface (Fig. 10.4). For moving sands, a new roughness parameter, k', is observed and may be approximated by height of ripples on the surface. This height ranges from 0.3 to 0.8 cm for sandy surfaces. The corresponding wind velocities, V_t, at height k' range from about 2.5 to 3.0 m/sec (Fig. 10.4).

To assess the sand-moving potential of winds recorded by meteorological stations, the wind velocity, v_t, at the height, z, of the recording instrument corresponding to the threshold wind velocity at height k', must be determined from a modification of equation (2) as follows:

$$v_t = 5.75\ V_* \log (z/k') + V_t \qquad (3)$$

Table 10.3 Sand-moving potential of winds. See text for description of parameters.

		k'	V_* (10 m)
Initiation of sand movement	(V_* = .22 m/sec)	0.3 cm	6.96 m/sec
		0.8 cm	6.92 m/sec
Maintenance of sand movement	(V_*'= .192 m/sec)	0.3 cm	6.39 m/sec
		0.8 cm	6.42 m/sec

where v_t is the threshold wind velocity at height z (10 m) and V_t is the threshold wind velocity at height k'. The results of these calculations for some cases are shown in Table 10.3. Although threshold wind velocities for sand movement as measured at 10 m range from 6 to 7.0 m/sec., other workers (Brookfield, 1970; McKee and others, 1977) have used the value 4.6 m/sec. To facilitate comparisons with previous studies, we also have chosen the same value. Possible errors arising from this choice will be discussed later.

Sand Drift Potential

Bagnold (1941) showed that the rate of sand transport, q, across a unit width is proportional to the cube of the dynamic threshold velocity, V_*', namely:

$$q = C \left(\frac{d}{D}\right) 1/2 \quad \frac{\rho f}{g} \quad V_*'^3 \tag{4}$$

where C is a constant related to the degree of sorting of the sand, and ranges from 1.5 for well-sorted sand to 2.8 for poorly-sorted sand; D is 0.25 mm, the diameter of "standard" sand; d is the average diameter of sand in the area studied; ρ_f is the fluid (air) density; and g is the acceleration of gravity.

The rate of sand transport can be calculated from meteorological observations by substitution of equation (3) into equation (4) as in the following steps:

$$q = Bv_e^3 \tag{5}$$

where $$B = C \left(\frac{0.174}{\log (z/k')}\right)^3 \left(\frac{d}{D}\right)^{1/2} \frac{\rho f}{g} \qquad (5a)$$

and $$v_e = (v - v_t) \qquad (5b)$$

v_e is the wind velocity in excess of the threshold velocity. The constant B is evaluated for several cases in Table 10.4. The amount of sand transported across a unit width, M, can be determined by multiplying the rate by the time wind is blowing, t, as follows:

$$M = qt = B(v - v_t)^3 t \qquad (6)$$

PROCEDURES OF COMPUTATION

Wind data were converted to computer readable files as matrices of direction and velocity, and ordered by month and station. All computations of sand-moving winds and sand drift potential were performed on these raw data.

Winds of velocities less than the threshold wind velocity, v_t, at the height of the anemometer are not capable of moving sand and, therefore, are excluded from consideration. Because the threshold wind velocity falls within a velocity class interval rather than dividing classes (Fig. 10.5), the frequency of occurrence in that particular class must be weighted according to where v_t falls within the

Table 10.4 Evaluation of the constant B for sand transport potential.

Sand Size	d(mm)	k'(cm)	C	/g	B (kg-sec^2/m^4)
well-sorted medium sand	.25	.3	1.5	1.25×10^{-6}	2.26
poorly-sorted medium sand	.25	.8	2.8	1.25×10^{-6}	6.21
well-sorted coarse sand	1	.3	1.5	1.25×10^{-6}	4.52
poorly-sorted coarse sand	1	.8	2.8	1.25×10^{-6}	12.4

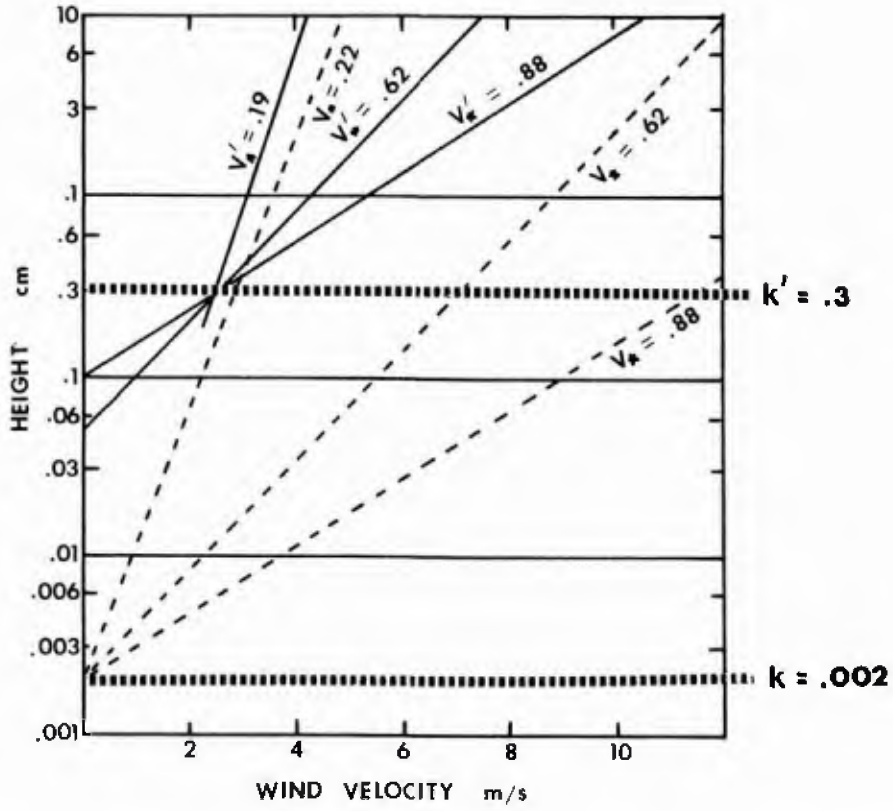

Figure 10.4 Plots illustrating relation of wind velocity to height. (See text for explanation).

interval. This assumes, probably unrealistically, that the frequencies of wind velocities are equally distributed within a given velocity interval. Most likely, this procedure tends to over estimate the frequency of sand-moving winds.

A similar sort of error arises from the compression of the data into fewer velocity classes as shown in Figure 10.5. Data originally summarized in nine velocity classes were compressed into five classes. Computation of frequency of sand-moving winds by the above method resulted in over-estimating their frequency by 20%. Wind distributions are commonly shown as circular histograms (wind roses) in which the arms are oriented in the direction from which the wind blows and their length is proportional to the frequency winds from that direction. The frequency of winds in each direction class, F_i, is:

$$F_i = \sum_{j=1}^{n} f_{i,j} \qquad (7)$$

where n is the number of velocity classes; and fi,j the frequency of winds in each direction-velocity "bin".

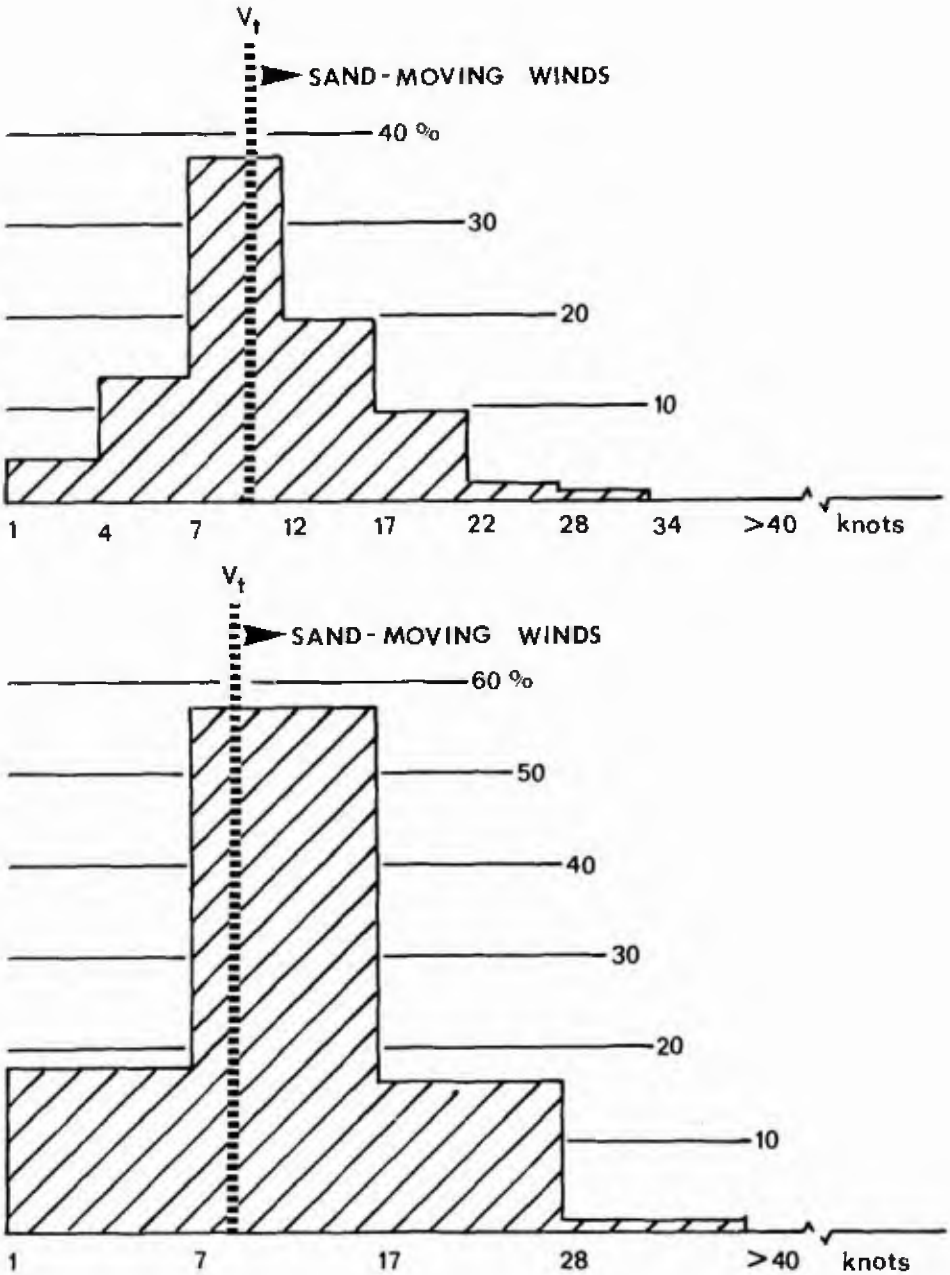

Figure 10.5 Cumulative graph of percentage of sand-moving winds as calculated in one station (Jeddah, number 24 in Figure 10.3 and in Table 10.1) during the month of January.

Wind roses may be constructed for sand-moving winds as well as for the total winds. Figure 10.6 illustrates the wind roses for all winds from stations in the Western Desert oases. Figure 10.7 shows the sand roses of the sand-moving winds in the same area covered by Figure 10.3. It is clear from this summary of the sand-moving winds in the Western Desert and adjacent regions that in the northern part of the desert a trend towards the southeast predominates. In the southern part of the desert, the trend of sand-moving winds is more toward the south.

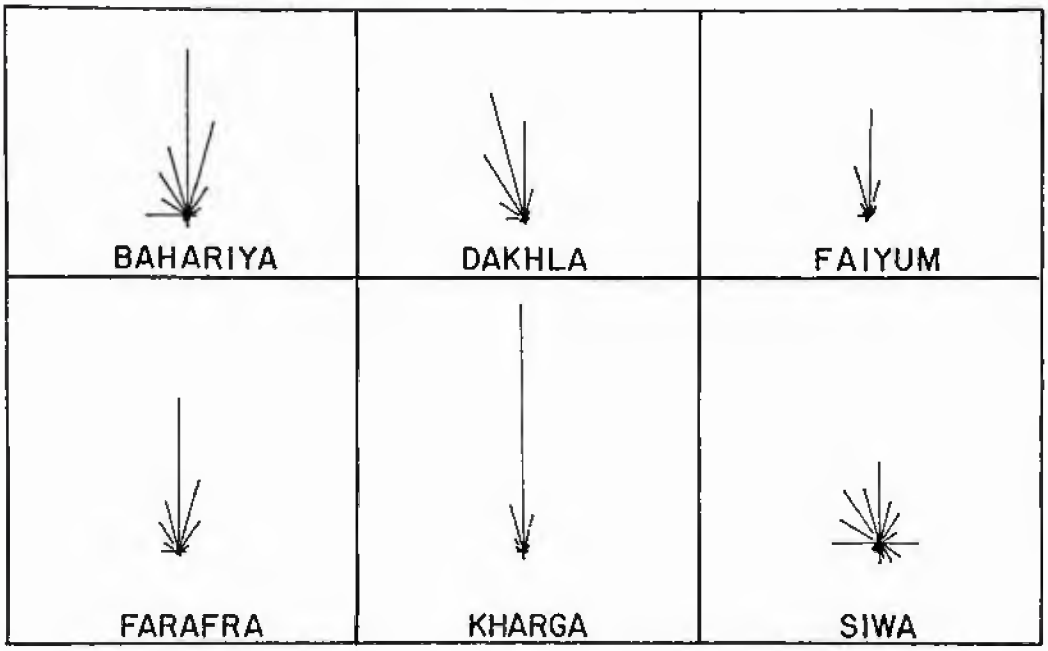

Figure 10.6 Annual summary of all winds in the six oases of the Western Desert of Egypt.

As shown previously, the potential for the drift of sand is proportional to the cube of sand-moving winds and their frequency. The sand drift potential, Pi, for a given direction is, therefore:

$$P_i \propto \sum_{j=1}^{n} (v - v_t)^3 f_{i,j} \qquad (8)$$

where v is taken as the mid-point of each velocity class, j. Errors may be expected to arise for the same reasons outlined above. These errors are compounded by cubing the velocities and are especially prone to arise from the nighest velocity class, for which there is no mid-point. Instead, an arbitrary "mid-point" is assumed, namely, 25.0 m/sec.

A summary of the sand drift potential in the studied area is shown in Figure 10.8. Comparisons of the directions in this figure with those in Figure 10.7 indicate that: (1) in the northern part of tne desert, the sand drift potential is more easterly than the direction of sand-moving winds; and (2) in the southern part of the Western Desert, both sand-moving winds and sand-drift potential point to the same direction. The direction in Figure 10.8 represent resultants, which were calculated as discussed below.

For comparison with eolian features and sand distribution patterns, the wind data (recalculated as sand drift potential) are more conveniently studied as resultant (or effective) directions, r, and magnitudes, m. These resultant directions and magnitudes are com-

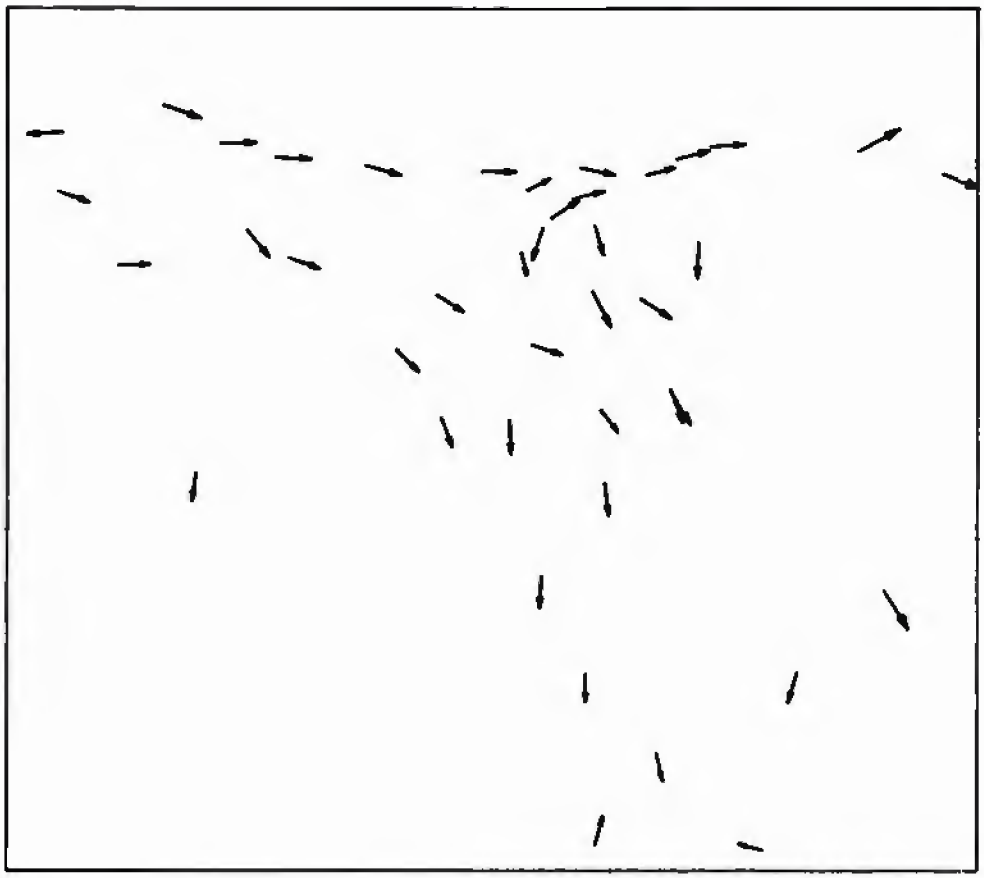

Figure 10.7 Annual summary of resultant winds at the stations shown in Figure 10.3.

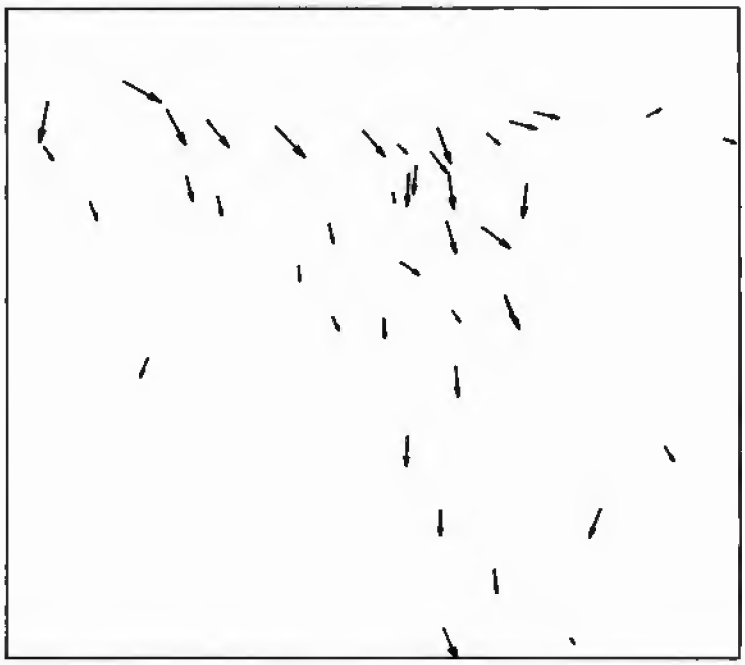

Figure 10.8 Annual summary of resultant sand drift potential at stations shown in Figure 10.3.

puted as the vector sums of frequency (sand drift potential) for each direction class by:

$$r = \tan^{-1}\left(\frac{\sum_{i=1}^{n} x_i \sin\theta_i}{\sum_{i=1}^{n} x_i \cos\theta_i}\right) + 180^{\circ} \qquad (9)$$

and

$$m = \left[\left(\sum_{i=1}^{n} x_i \sin\theta_i\right)^2 + \left(\sum_{i=1}^{n} x_i \cos\theta_i\right)^2\right]^{1/2} \qquad (10)$$

where x_i is either the total of frequencies, or the drift potential for direction class, i, of n classes. The angle (in E-N coordinates) is the lower limit of each direction class.

Meteorological stations are scattered in the study region and are sparse in the area of most interest, the Western Desert (Fig. 10.3). This makes the patterns of wind and drift potential difficult to interpret. To alleviate this drawback, a regular, rectangular grid of points was overlaid on the region and values of direction and magnitude were interpolated from the locations of meteorological stations to the grid points. The computational procedure for this interpolation is the simple algorithm described by Davis (1973).

Essentially, the value at a given grid point is the average of the nearest n values (we chose n=6) weighted by the inverses of their distances from the grid point. The value, M_k, at a grid point is given by:

$$M_k = \frac{\sum_{i=1}^{6} (M_i/D_{ik})}{\sum_{i=1}^{6} (1/D_{ik})} \qquad (11)$$

where M_i is the value at one of the 5 nearest neighbors and D_{ik} is the Euclidean distance from that point to the grid point determined by:

$$D_{ik} = \left[(x_i - x_k)^2 + (y_i - y_k)^2\right]^{1/2} \qquad (12)$$

where x_i and x_k are the x-coordinates (longitude) of the station and grid point, respectively; and y_i and y_k the y-coordinates (latitude).

To interpolate orientations, two values were computed for each grid point, namely:

$$S_k = \frac{\sum_{i=1}^{6}(\sin\theta_i/D_{ik})}{\sum_{i=1}^{6}(1/D_{ik})} \qquad (13a)$$

and

$$C_k = \frac{\sum_{i=1}^{6}(\cos\theta_i/D_{ik})}{\sum_{i=1}^{6}(1/D_{ik})} \qquad (13b)$$

where D_{ik} is as previously defined and is the resultant vector orientation at station i. The orientation of a grid point, is then:

$$\theta_k = \tan^{-1}\left(\frac{S_k}{C_k}\right) \qquad (14)$$

The general flow pattern of wind in the study area is shown in Figure 10.9 as annual summary of sand drift potential streamlines. This pattern clearly established the westerly flow of wind along the Mediterranean seacoast, which continues eastwards into the Arabian Peninsula. In the northern part of the Western Desert, the streamline wind flow pattern is to the south-southeast. In the rest of the desert the flow pattern is basically to the south. The veering to the

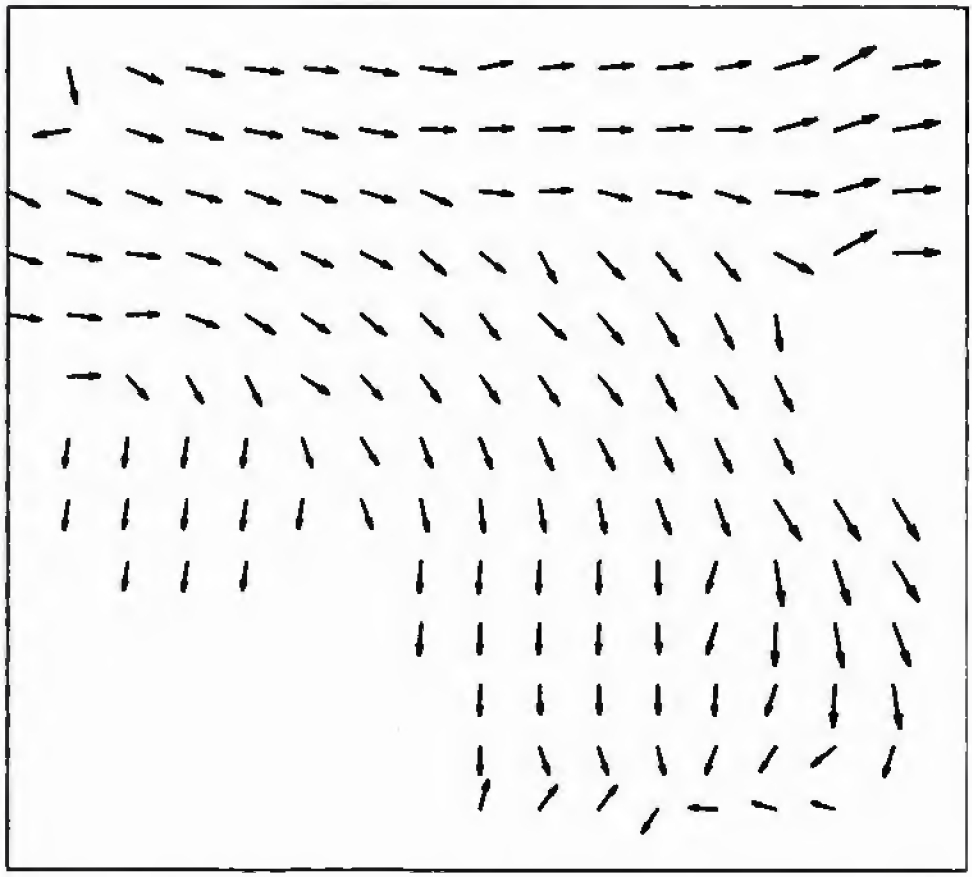

Figure 10.9 Streamlines of annual summary of resultant sand drift potential developed by trend surface analysis of data shown in Figure 10.8.

southwest near the convergence of the borders of Egypt, Libya and Sudan, which is displayed in the sand dune patterns (Fig. 10.10), is not indicated in these streamlines.

COMPARISONS WITH EOLIAN FEATURES

If we compare the annual summaries of sand drift potential in resultants (Fig. 10.8) with the orientation of dunes (Fig. 10.9) in the Western Desert of Egypt, numerous conflicts appear. Among these are:

1. In the north, the sand drift potential is basically to the east, while the dunes of Qattara are oriented in a southeasterly direction. This may be due to the fact that wind stations are placed in towns along the seacoast and reflect only the Mediterranean Sea system of winds, which may have little to do with the sand-moving winds inland.

2. In the central part of the desert, annual summaries of the sand drift potential are also more easterly than the dune orientations. This is most likely due to the fact that wind stations are in oases within depressions, which locally affect wind directions as discussed below.

Figure 10.10 Landsat image showing the deflection of dune bundles by topographic highs at the border intersection between Egypt, Libya and Sudan (E-2398-08044).

3. In the southern part of the desert, particularly the southwestern part, little correlation can be made, because of the lack of meteorological stations southwest of Kharga Oasis.

This shows that annual resultants of sand transport potential of the winds should not be used to establish dune orientation. Results of such correlations may be misleading. However, when the data are generalized by interpolation to produce annual summaries of sand drift potential streamlines (Fig. 10.9), the correlations of sand dunes in the Western Desert of Egypt (Fig. 10.1), correlate better with such streamlines.

RELATIONSHIP OF WIND DIRECTION TO LOCAL TOPOGRAPHIC SETTING

The Western Desert of Egypt is basically a rocky plain which slopes gently to the north. The Uweinat Mountain and the Gilf Kebir plateau in the southwest corner constitute the only prominences that are higher than 1900 m above sea level. The central and southern parts of the desert average 200 to 500 m in elevation, and rocks of the northern belt are less than 200 m above sea level. The generally flat plateau desert of sedimentary rocks is broken by seven major depressions including the Qattara and those that enclose the oases of

Siwa, Faiyum, Bahariya, Farafra, Dakhla, and Kharga (Fig. 10.1). Summaries of wind directions based on data from meteorological stations in the six oases are given in Figure 10.6.

Qattara Depression

The Qattara Depression is the largest of the Western Desert depressions and occupies approximately 19,500 km^2, or 1/15 the land area of Egypt. This depression also contains the lowest point on the continent of Africa, being 134 m below sea level. Much like other depressions in the Western Desert, its northern borders are clearly marked by a distinct scarp, whereas the depression grades into the terrain to the south (El-Baz, 1979b). The dunes of Qattara emanate from its southern part as bundles of longitudinal dunes that taper to the southeast (Fig. 10.1). This direction reasonably agrees with the inferred sand transport directions in Figure 10.8. Agreement between the orientation of dunes and inferred wind direction is probably due to the fact that southern Qattara can be considered an open plain, without scarps or other topographic barriers to affect wind circulation.

Siwa Depression

The Siwa depression is irregularly-shaped and generally elongate in an east-west direction. It is the farthest depression from the Nile Valley and is approximately 50 km long and covers 300 km^2; parts of it are 60 m below sea level. About 15 km east of the Siwa depression is another depression about two-thirds its size (El-Baz, 1979c). Both depressions are bounded by faults that intersect in an "X" pattern. The southern borders of the Siwa Oasis blend with the northern boundary of the Great Sand Sea. Near Siwa, the dunes of this sand mass are sinuous and appear to have formed under varying wind regimes as suggested by the wind directions in Figure 10.6. However, yardangs along the western borders of the depression are all oriented in an east-west direction. This may have resulted from both structural control and strength of local winds from the west (Mediterranean wind system).

Faiyum Depression

The Faiyum depression is closest to the Nile Valley and occupies a circular area of approximately 1,700 km^2, much of which lies below sea level. The limestone cliffs of the Faiyum depression confine bundles of complex barchan chains. These dunes appear to be shifting in a south-southeast direction (Fig. 10.1). Some have reached the western borders of the fertile Nile Valley and have started encroaching on its agricultural land (El-Baz, 1979b). The alignment of the dunes along the scarp indicates the effect of that scarp in dividing the sand carrying wind towards the south rather than to the southeast (Fig. 10.1).

Bahariya Depression

The Bahariya depression is spindle-shaped and is elongate in a

northeast direction. It is approximately 95 km long and 45 km wide and covers an area of 1,800 km^2. The escarpment that completely encircles the depression is approximately 100 m high. The depression is unique among others in the Western Desert in that hills form a discontinuous line in its center. These hills appear to affect the local wind regime in the Bahariya depression as shown in Figure 10.6.

Farafra Depression

The Farafra depression is roughly triangular in shape and is bounded by high scarps on the east and west and a low scarp on the north. It is open towards the south where it meets the Dakhla escarpment some 200 km away. Most of the exposed rock in the depression is chalk of Maastrichtian age (Said, 1962). The eastern half of the depression is covered by dune sand. Field observations indicate that this sand mass is similar to that of the Great Sand Sea. The large dunes are gently sloping whaleback dunes, several kilometers across. Superposed on these dunes are sharp-crested, partly sinuous longitudinal dunes (El-Baz, 1979b). There is a small field of dunes that is enclosed in a small depression in the northern part of the larger Farafra depression. The dunes in this small field are oriented in the same direction as the scarps, approximately N 50°E (Manent and El-Baz, 1980).

Dahkla Depression

The Dakhla depression lies south of an escarpment that trends west-northwest from Kharga for approximately 250 km. South of the escarpment, the exposed rock belongs to the Nubian Sandstone, which covers most of the southern half of the Western Desert. The Dakhla

Figure 10.11 Landsat image showing dunes oriented in a NW-SE direction in the upper right corner and more southerly in the Kharga depression in the lower left corner (E-1110-07561).

depression is connected to the Kharga depression by level ground south of a large, arcuate escarpment known as the Abu Tartur Plateau. The wind pattern in the Dakhla depression appears to be identical to that of Kharga (Fig. 10.6). Because the Dakhla depression is open to the south, there are little if any topographic effects on wind direction and orientation of dunes.

Kharga Depression

The Kharga depression (Fig. 10.11) is aligned in a north-south direction. The succession of rocks from the floor upward begins with Nubian Sandstone, which is overlain by purple and varigated shales, phosphatic beds, Dakhla shale, chalk, Esna shales, Thebes limestone, and travertine and loess on top (Said, 1962). The depression is open to the south and southwest. The width of the depression varies from 20 km in the north to 80 km in the south. Within the depression numerous bundles of active barchans and barchan chains hamper the agricultural development of the land (El-Baz, 1979b). Hence, the effect on dune orientation of the north-south trending scarp on the eastern side of the depression are quite obvious (Fig. 10.1). North and east of the depression, the dunes point to the southeast, but within Kharga, they move due south.

Gilf Kebir and Uweinat

Beyond Kharga, and southwest of the other oases, the terrain of the Western Desert is flat to undulating; it is interrupted by a few topographic highs particularly in the southwestern corner (El-Baz and Maxwell, 1979a). The effects of the Gilf Kebir plateau and Uweinat Mountain on dune orientations are clearly visible on Earth orbital photographs (Fig. 10.10). However, the exact wind directions are not known because of the lack of recording stations in southwestern Egypt.

AUTOMATED METEOROLOGICAL STATIONS

As previously stated, a full understanding of the wind regime in the Western Desert is hampered by the lack of meteorological stations in the open desert. The present stations are located within depressions, and there are no stations in the southwestern part of the desert. This deficiency may be remedied by utilizing automated meteorological stations.

Space age technology has provided a wide variety of sensing devices that can, for example, measure air and water quality, monitor the flow within a pipeline, or detect earthquakes. It has recently been proposed that the same kind of technology be applied to monitoring climatic and meteorological conditions in remote desert regions (El-Baz, 1979d). Automated stations can obtain the measurements, average them over a period of time, and relay them to orbiting satellites. The satellites, in turn, can beam these data to Earth for analysis and synthesis.

A meteorological data collection scheme may use Earth orbiting satellites to relay data from a number of automated stations to one or

more receiving sites. There are three basic elements to such a scheme: 1) a data collection platform (DCP) connected to the sensor recorders; 2) a radio transponder with receiving and transmitting capabilities on board a satellite; and 3) a data receiving station for retrieval, processing, and dissemination of the collected data.

There are two experimental programs that utilize such a system for meteorological monitoring. These are for use in remote places that represent extremes of Earth weather: the perpetual ice sheets of Antarctica (T. Howard, pers. comm.) and the sun-scorched deserts of the American southwest (J. F. McCauley, pers. comm.).

Based on the above, it is recommended that testing of this method of meteorological monitoring via orbiting satellites be conducted in the western Desert of Egypt. The desert is ideal for this type of research, because "the free interplay of sand and wind has been allowed to continue for a vast period of time, and here, if anywhere, it should be possible in the future to discover the laws of sand movement, and the growth of dunes" (Bagnold, 1933, p. 121).

CONCLUSIONS

1. The general clockwise wind circulation pattern noted by Bagnold (1933) in the Western Desert of Egypt is supported by study of dune orientations from space images and photographs.

2. Annual wind summaries and sand drift potentials based on these summaries do not provide the same directions as those of the dunes. Generalizations by interpolation between stations correlate better with dune orientations.

3. Differences between directions of sand-moving potential and the dunes may be due to local topographic effects on the wind.

4. Depressions that are bound by north-south escarpments such as Faiyum and Kharga impose the same alignment of the dunes within these depressions.

5. Topographic highs such as the Gilf Kebir plateau and the Uweinat Mountain in the southwestern part of the desert also affect dune orientations, where the winds change directions to skirt these highs.

6. To fully understand the wind regime of the Western Desert, automated meteorological stations should be emplaced in the open desert, particularly in its southwestern parts.

REFERENCES

Bagnold, R. A., 1933, A further journey through the Libyan desert :Geogr. Jour., v. 82, p. 103-129 and 211-235.

———, 1941, The Physics of Blown Sand and Desert Dunes: Methuen and Co. Ltd., London, 265 p.

Bagnold, R. A., Peel, R. F., Myers, O. H., and Winkler, H. A., 1939, An Expedition to the Gilf Kebir and Uweinat, 1938; Geogr. Jour., v. 93, p. 281-313.

Brookfield, M., 1970, Dune trends and wind regime in Central Australia: in Ann. Geomorph. Suppl. 10 Piedmont Plains and Sand Formations in Arid and Humid Tropic and Subtropic Regions, p. 121-153.

Davis, J. C.,1973, Statistics and Data Analysis in Geology: New York, Wiley, 550 p.

El-Baz, F., 1979b, The Western Desert of Egypt, its problems and potentials: in Bishay, A. and McGinnes, W. G., eds., Advances in Desert and Arid Land Technology and Development, v. 1, Harwood Academic Pub., p. 67-84.

———, 1979c, Siwa: Resort of kings: Aramco World, v. 30, no. 4, p. 30-35.

———, 1979d, Monitoring the desert environment from space: in Bishay, A. and McGinnes, W. G., eds., Advances in Desert and Arid Land Technology and Development, v. 1, New York, Harwood Academic Pub., p. 383-398.

El-Baz, F. and Maxwell, T. A., 1979a, Eolian streaks in southwestern Egypt and similar features in the Cerberus region of Mars: Proc. Lunar and Planetary Science Conf., 10th, New York, Pergamon, p. 3017-3030.

Gifford, A. W., Warner, D, M., and El-Baz, F., 1979, Orbital observations of sand distribution in the Western Desert of Egypt: in El-Baz, F. and Warner, D. M., eds., Apollo-Soyuz Test Project Summary Science Report, Volume II: Earth Observations and Photography: NASA SP-412, Wash. D. C., p. 219-236.

Griffiths, J. F. and Soliman, K. H., 1972, The northern desert (Sahara): in Griffiths, J. F., ed., Climates of Africa: Amsterdam, Elsevier, 604 p.

Henning, D. and Flohn, H., 1977, Climate Aridity Index Map: U. N. Conference on Desertification, UNEP, Nairobi, Kenya.

Manent, L. S. and El-Baz, F., 1980, Effects of topography on dune orientation in the Farafra region, Western Desert of Egypt, and implications to Mars: in Reports of Planetary Geology Program - 1980, NASA TM-82385, Wash. D. C., p. 298-300.

McKee, E. D., Breed, C. S., and Fryberger, S. G., 1977, Desert sand seas: in Skylab Explores the Earth: NASA SP-380, Wash. D. C., p. 5-47.

Ownbey, J. W., 1978, Guide to Standard Weather Summaries and Climatic Services: National Tech. Information Service, Wash. D.C., AD-A047482.

Said, R., 1962, The Geology of Egypt: Amsterdam, Elsevier Pub. Co., 377 p.

Wolfe, R. W. and El-Baz, F., 1979, The wind regime of the Western Desert of Egypt (abstract): in Reports of Planetary Geology Program, 1978-1979: NASA Tech. Memorandum 80339, Wash. D. C., p. 299-301.